ELSEVIER

PII: S0141-1187(96)00019-3

Applied Ocean Research **18** (1996) 1–11

0141-1187/96/$15.00

Water waves incident on an infinitely long rectangular inlet

Robert A. Dalrymple
Center for Applied Coastal Research, University of Delaware, Newark, DE 19716, USA

&

P. A. Martin
Department of Mathematics, University of Manchester, Manchester M13 9PL, UK

(Received 16 April 1996)

Obliquely incident linear wave trains encountering an inlet on a straight reflecting shoreline are examined to determine the response of the inlet to the wave forcing. The problem is separated into a symmetric problem and an antisymmetric problem, with respect to the channel centerline. Fourier transforms are used to solve the Helmholtz equation in the ocean and an eigenfunction expansion is used in the channel (which has constant depth and a rectangular cross-section). Matching conditions at the mouth of the inlet provide the matrix equation to be solved for the amplitudes of the wave motions. The amplitudes of the symmetric and antisymmetric wave modes are provided as a function of dimensionless channel width and angle of incidence. Plane wave and long wave approximations are also provided. Copyright ©1996 Elsevier Science Limited

1 INTRODUCTION

Water waves encountering entrance channels present an interesting problem as the waves undergo reflection, refraction, diffraction and shoaling due to shorelines, shoals, jetties, tidal currents, and a variable depth channel.

Melo & Guza,[1,2] through field and numerical means, showed that a tidal inlet comprised of rubblemound jetties absorbs a considerable amount of the wave energy entering the inlet from the ocean in the porous inlet sidewalls. Dalrymple[3] developed a simple model to explain this behavior using a simple eigenfunction expansion of the waves in the channel (assuming a rectangular channel cross-section) and an impedance boundary condition at the sidewalls. Dalrymple assumed that the waves at the mouth of the inlet had a constant amplitude and phase; that is, they were planar and normally incident. One consequence of this assumption and the impedance boundary condition was a fictitious amplification of the waves occurring within one wavelength of the channel mouth. Martin & Dalrymple[4] analytically examined the interaction of waves and porous sidewalls, providing proof of the analogy of wave propagation in a channel with absorbing sidewalls and a breakwater gap (Peregrine, as cited by Melo & Guza).

Recently, Kirby *et al.*[5] and Dalrymple *et al.*[6] have examined the propagation of waves in inlets with variable plan form, such as diverging or curved channels. In both of these cases as well, the wave form at the mouth of the channel was assumed to be a normally incident plane wave train (in Cartesian coordinates).

Here we examine the interaction between obliquely incident wave trains in the ocean and an inlet embedded in a perfectly reflecting shoreline. The inlet will be assumed to be infinitely long; any reflected waves occurring due to a realistic finite length inlet channel are assumed to be negligible due to the strong damping referred to above. Our idealized inlet has a rectangular cross-section of the same depth as the ocean and has perfectly reflecting sidewalls. Momoi[7–10] has treated normally incident long waves for this case (with increasing orders of approximation), using three separate domains with an eigenfunction expansion in each. The domains are an outer region in the ocean, a 'buffer' region consisting of a semicircular domain in front of the channel, and the channel itself. Here we use two domains (with an eigenfunction expansion in one and an integral representation in the other) and include obliquely incident short waves.

Eigenfunction expansions have long played a role in

water wave problems, particularly for problems that involve matching between two domains of different depths. Takano[11] treated a step discontinuity using eigenfunction expansions over the depth (z direction) in each domain of constant water depth. Newman[12] examined waves propagating in an infinitely deep ocean connnected to a finite depth shelf, expressing the wave motion in terms of Havelock's[13] integral solution for a wavemaker in deep water and an eigenfunction expansion in the shallower region. Eigenfunctions expansions in the lateral direction (y in our case) have been used, for example, by Dalrymple and Martin[14] for waves past a series of offshore breakwaters, and in fact lead to the angular spectrum model of water waves (see Dalrymple and Kirby[15]).

In the next section, we separate the incident wave field into a problem symmetric about the channel centerline and an antisymmetric problem. Each of these problems is then solved by the use of Fourier transforms in the cross-channel direction. Combining the two solutions then provides the total wave field for arbitrary channel width to water wave length. The advantage of the eigenfunction solution is that the near-field behavior of the wave field is easily obtained. As alternatives, plane wave (only one cross-channel eigenfunction) and long wave asymptotic solutions are also obtained and compared to the full eigenfunction solution and to another asymptotic solution obtained recently by McIver & Rawlins.[16] In Section 3, the amplitudes of the various Fourier modes are shown as a function of incident angle and dimensionless channel width. The total energy propagating down the channel as a function of the channel geometry and wave angle of incidence is also computed.

The water wave problem is a two-dimensional analog to the acoustics, electromagnetics, or optics problem of waves entering an infinite slot. Many early solutions have used variational principles (Miles[17]) or a single dominant mode (Chester[18]). Modal expansions have been used recently; see, for example, Scharstein[19] in connection with an integral approach, or Kabalan and El-Haji,[20] using a matrix method similar to ours (both of these papers are in the field of electromagnetics). Here, a modal expansion is used to provide a more detailed examination of the wave field in the vicinity of the duct. One important result is the reduction of the area integrals, as required for the solution of the modal amplitudes, into line integrals.

2 THEORETICAL CONSIDERATIONS

The ocean will be considered as the half-plane, $x < 0$ with a reflecting shoreline at $x = 0$, except at the mouth of the channel, which is located on the y axis, $-b < y < b$, thus the channel centerline corresponds to the $+x$ axis. The velocity potential governing the linear wave motion in the constant depth ocean satisfies the Helmholtz equation and can be written as

$$\Phi_1(x, y, z, t) = \mathrm{Re}\left\{\phi_1(x, y)\frac{\cosh k(h+z)}{\cosh kh}\,\mathrm{e}^{-\mathrm{i}\omega t}\right\}$$

where k and ω are related by the dispersion relationship:

$$\omega^2 = gk\tanh kh$$

We decompose ϕ_1 as

$$\phi_1 = \phi_{\mathrm{inc}} + \phi_{\mathrm{ref}} + \phi_1^{\mathrm{s}} + \phi_1^{\mathrm{a}}$$

where

$$\phi_{\mathrm{inc}} = p\,\mathrm{e}^{\mathrm{i}k(y\sin\theta + x\cos\theta)}$$

gives the incident wave, scaled by the (dimensional) constant p, propagating at an angle θ to the x-axis,

$$\phi_{\mathrm{ref}} = p\,\mathrm{e}^{\mathrm{i}k(y\sin\theta - x\cos\theta)}$$

gives the reflected wave, and $\phi_1^{\mathrm{s}} + \phi_1^{\mathrm{a}}$ gives the wave radiating out of the channel due to the interaction of the incident waves and the channel. Rearranging $\phi_{\mathrm{inc}} + \phi_{\mathrm{ref}}$ yields two different standing waves:

$$\phi_{\mathrm{inc}} + \phi_{\mathrm{ref}} = 2p\cos(ky\sin\theta)\cos(kx\cos\theta) + 2\mathrm{i}p\sin(ky\sin\theta)\cos(kx\cos\theta) \quad (1)$$

The first standing wave pattern is symmetric about the x axis and the second is antisymmetric. Therefore, we split the problem into two: one symmetric and the other antisymmetric. Here, and below, we identify the symmetric wave fields with a superscript 's' and the antisymmetric fields with a superscript 'a'. Thus, we can use the following Fourier integral representations for the symmetric and antisymmetric problems respectively:

$$\phi_1^{\mathrm{s}} = \frac{1}{\pi}\int_0^\infty A^{\mathrm{s}}(\lambda)\,\mathrm{e}^{-\mathrm{i}\beta(\lambda)x}\cos\lambda y\,\mathrm{d}\lambda \quad (2)$$

$$\phi_1^{\mathrm{a}} = \frac{1}{\pi}\int_0^\infty A^{\mathrm{a}}(\lambda)\,\mathrm{e}^{-\mathrm{i}\beta(\lambda)x}\sin\lambda y\,\mathrm{d}\lambda \quad (3)$$

for $x < 0$, where

$$\beta(\lambda) = \begin{cases}\sqrt{k^2-\lambda^2}, & 0 \le \lambda \le k\\ \mathrm{i}\sqrt{\lambda^2-k^2}, & \lambda > k.\end{cases} \quad (4)$$

The forms of $A^{\mathrm{s}}(\lambda)$ and $A^{\mathrm{a}}(\lambda)$ are to be determined by matching to the wave solution in the channel.

Within the channel of width $2b$, the wave potential is

$$\Phi_2(x, y, z, t) = \mathrm{Re}\left\{\phi_2(x, y)\frac{\cosh k(h+z)}{\cosh kh}\,\mathrm{e}^{-\mathrm{i}\omega t}\right\}$$

where $\phi_2 = \phi_2^{\mathrm{s}} + \phi_2^{\mathrm{a}}$,

$$\phi_2^{\mathrm{s}} = \sum_{n=0}^\infty a_n^{\mathrm{s}}\,\mathrm{e}^{\mathrm{i}\beta(\lambda_n^{\mathrm{s}})x}\cos\lambda_n^{\mathrm{s}} y \quad (5)$$

$$\phi_2^{\mathrm{a}} = \sum_{n=0}^\infty a_n^{\mathrm{a}}\,\mathrm{e}^{\mathrm{i}\beta(\lambda_n^{\mathrm{a}})x}\sin\lambda_n^{\mathrm{a}} y \quad (6)$$

for $x > 0$, $-b < y < b$,

$$\lambda_n^{\mathrm{s}} = n\pi/b \quad \text{and} \quad \lambda_n^{\mathrm{a}} = (n+\tfrac{1}{2})\pi/b$$

The first term in the summation (5) represents a wave propagating directly down the straight channel; the remaining terms in (5) and all the terms in (6) are waves which propagate down the channel obliquely, reflecting from the vertical side walls. For values of n such that $\lambda_n^s > k$ or $\lambda_n^a > k$, these waves decay in the x-direction; see (4).

To determine the functions A^s and A^a, and the coefficients a_n^s and a_n^a, two matching conditions are used. The first is the continuity of the velocities in the x-direction across the mouth of the channel,

$$\frac{\partial \phi_2}{\partial x} = \frac{\partial \phi_1}{\partial x} \quad \text{at } x = 0,\ |y| < b \tag{7}$$

The second is the requirement that the water surface be continuous across the channel mouth, which can be expressed as a matching of the velocity potentials:

$$\phi_2 = \phi_1 \quad \text{at } x = 0,\ |y| < b \tag{8}$$

In addition, there is the reflecting-shoreline condition,

$$\frac{\partial \phi_1}{\partial x} = 0 \quad \text{at } x = 0,\ |y| > b \tag{9}$$

To proceed, it is convenient to solve the symmetric and antisymmetric problems separately; it is sufficient to consider $y > 0$.

2.1 Symmetric problem

Combining (9) with the first matching condition, (7), leads to

$$-\frac{\mathrm{i}}{\pi}\int_0^\infty A^s(\lambda)\beta(\lambda)\,\cos\lambda y\,\mathrm{d}\lambda = \begin{cases} \displaystyle\sum_{n=0}^{\infty} \mathrm{i}a_n^s\beta(\lambda_n^s)\,\cos\lambda_n^s y & \text{for } 0 \le y \le b \\ 0 & \text{for } y > b \end{cases} \tag{10}$$

We can solve for $A^s(\lambda)$ by inverting the Fourier cosine transform:

$$A^s(\lambda) = -\sum_{n=0}^{\infty} a_n^s \frac{\beta(\lambda_n^s)}{\beta(\lambda)}\,\mathcal{L}_n^s(\lambda) \tag{11}$$

where

$$\mathcal{L}_n^s(\lambda) = 2\int_0^b \cos\lambda_n^s y\,\cos\lambda y\,\mathrm{d}y = \frac{2(-1)^n\lambda\sin\lambda b}{\lambda^2 - (\lambda_n^s)^2} \tag{12}$$

Note that $\mathcal{L}_n^s(\lambda)$ is well defined for all values of λ; in particular,

$$\epsilon_n \mathcal{L}_n^s(\lambda_n^s) = 2b$$

where $\epsilon_0 = 1$ and $\epsilon_m = 2$ for $m > 0$.

Substitute $A^s(\lambda)$ from (11) into (2), and then use the second matching condition (8) to obtain

$$\sum_{n=0}^{\infty} a_n^s \cos\lambda_n^s y = 2p\cos(kx\sin\theta) - \frac{1}{\pi}\sum_{n=0}^{\infty} a_n^s\beta(\lambda_n^s)\int_0^\infty \mathcal{L}c_n^s(\lambda)\,\cos\lambda y\frac{\mathrm{d}\lambda}{\beta(\lambda)} \qquad 0 \le y < b$$

Using the orthogonality of $\{\cos\lambda_n^s y\}$ over the range $0 \le y \le b$ removes the y dependency and provides equations for a_m^s:

$$ba_m^s = \epsilon_m p\,\mathcal{L}_m^s(k\sin\theta) - \tfrac{1}{2}\epsilon_m\sum_{n=0}^{\infty} a_n^s\beta(\lambda_n^s)\,D_{mn}^s \text{for } m = 0, 1, 2, \ldots \tag{13}$$

The term D_{mn}^s is defined by

$$D_{mn}^s = D_{nm}^s = \frac{1}{\pi}\int_0^\infty \mathcal{L}_m^s(\lambda)\,\mathcal{L}_n^s(\lambda)\,\frac{\mathrm{d}\lambda}{\beta(\lambda)}; \tag{14}$$

its evaluation is discussed in Appendix A. Rearranging and truncating the summation to only $N + 1$ terms gives

$$\sum_{n=0}^{N} a_n^s\,(2b\delta_{mn} + \epsilon_m\beta(\lambda_n^s)\,D_{mn}^s) = 2p\,\epsilon_m\mathcal{L}_m^s(k\sin\theta) \text{for } m = 0, 1, 2, \ldots, N \tag{15}$$

where $\delta_{mn} = 1$ for $m = n$ and is zero otherwise. Equation (15) is an $(N + 1) \times (N + 1)$ matrix equation for a_m^s; it is solved by standard methods.

2.2 Antisymmetric problem

We proceed as in Section 2.1. Combining (9) with (7), and inverting the Fourier sine transform gives

$$A^a(\lambda) = -\sum_{n=0}^{\infty} a_n^a \frac{\beta(\lambda_n^a)}{\beta(\lambda)}\,\mathcal{L}_n^a(\lambda) \tag{16}$$

where

$$\mathcal{L}_n^a(\lambda) = 2\int_0^b \sin\lambda_n^a y\,\sin\lambda y\,\mathrm{d}y = \frac{2(-1)^{n+1}\lambda\cos\lambda b}{\lambda^2 - (\lambda_n^a)^2} \tag{17}$$

$\mathcal{L}_n^a(\lambda)$ is also well defined for all values of λ, including λ_n^a, as $\mathcal{L}_n^a(\lambda_n^a) = b$.

Substituting for $A^a(\lambda)$ from (16) into (3), followed by use of the second matching condition (8) and the orthogonality of $\{\sin\lambda_n^a y\}$ over the range $0 \le y \le b$, gives

$$ba_m^a = 2ip\mathcal{L}_m^a(k\sin\theta) - \sum_{n=0}^{\infty} a_n^a\beta(\lambda_n^a)\,D_{mn}^a \text{for } m = 0, 1, 2, \ldots \tag{18}$$

where

$$D_{mn}^a = D_{nm}^a = \frac{1}{\pi}\int_0^\infty \mathcal{L}_m^a(\lambda)\,\mathcal{L}_n^a(\lambda)\,\frac{\mathrm{d}\lambda}{\beta(\lambda)}; \tag{19}$$

the evaluation of D^{a}_{mn} is discussed also in Appendix A. Rearranging and truncating to N terms as before, we obtain

$$\sum_{n=0}^{N} a_n^{a}\left(b\delta_{mn} + \beta(\lambda_n^{a})D_{mn}^{a}\right) = 2ip\,\mathcal{L}_m^{a}(k\sin\theta) \quad \text{for } m = 0, 1, 2, \ldots, N \tag{20}$$

which is an $(N+1)\times(N+1)$ matrix equation for a_m^{a}.

2.3 Alternative formulation

An alternative formulation is possible. From (11) and (16), we can see that the functions $A^{s}(\lambda)$ and $A^{a}(\lambda)$ are even and odd, respectively. Hence, we can combine (2) and (3) to give

$$\phi_1 = \phi_{inc} + \phi_{ref} + \frac{1}{2\pi}\int_{-\infty}^{\infty} A(\lambda)\,e^{-i\beta(\lambda)x}\,e^{i\lambda y}\,d\lambda, \quad x < 0 \tag{21}$$

where

$$A(\lambda) = A^{s}(\lambda) - iA^{a}(\lambda) \tag{22}$$

The third term in (21) is a Fourier integral representation for the radiated waves. From (12) and (17), we can write $\mathcal{L}_n^{s}$ and $\mathcal{L}_n^{a}$ as Fourier transforms:

$$\mathcal{L}_n^{s}(\lambda) = \int_{-b}^{b} \cos\lambda_n^{s} y\,e^{-i\lambda y}\,dy$$

$$\mathcal{L}_n^{a}(\lambda) = -i\int_{-b}^{b} \sin\lambda_n^{a} y\,e^{-i\lambda y}\,dy$$

If we now substitute for $A(\lambda)$ into (21), using (11), (16) and the convolution theorem for Fourier transforms, we obtain

$$\begin{aligned}\phi_1 = \phi_{inc} + \phi_{ref} &- \frac{1}{2}\sum_{n=0}^{\infty} a_n^{s}\beta(\lambda_n^{s}) \times \int_{-b}^{b} H_0^{(1)}\left(k\sqrt{x^2+(y-\zeta)^2}\right)\cos\lambda_n^{s}\zeta\,d\zeta \\ &- \frac{1}{2}\sum_{n=0}^{\infty} a_n^{a}\beta(\lambda_n^{a}) \times \int_{-b}^{b} H_0^{(1)}\left(k\sqrt{x^2+(y-\zeta)^2}\right)\sin\lambda_n^{a}\zeta\,d\zeta\end{aligned} \tag{23}$$

Here, we have used the known representation

$$H_0^{(1)}\left(k\sqrt{x^2+y^2}\right) = \frac{1}{\pi}\int_{-\infty}^{\infty} \frac{e^{-i\beta(\lambda)x}e^{i\lambda y}}{\beta(\lambda)}\,d\lambda, \quad x < 0$$

for the Hankel function, $H_0^{(1)}$; see, for example, Chester[18] or Dalrymple & Greenberg.[21] The last two terms on the right-hand side of (23) represent the waves scattered by the inlet in the ocean. Each Fourier mode (corresponding to $n = 0, 1, \ldots$) in the channel acts as a wavemaker, creating a radially spreading ocean wave, similar to that discussed by Dalrymple and Greenberg. Note that we can write (23) as

$$\phi_1 = \phi_{inc} + \phi_{ref} + \frac{i}{2} \times \int_{-b}^{b} \frac{\partial\phi_2}{\partial x}(0,\zeta)H_0^{(1)}\left(k\sqrt{x^2+(y-\zeta)^2}\right)d\zeta; \tag{24}$$

this formula could have been obtained directly by applying Green's theorem in the ocean to the radiated field, $\phi_1 - \phi_{inc} - \phi_{ref}$, and

$$H_0^{(1)}\left(k\sqrt{(x-\xi)^2+(y-\zeta)^2}\right) + H_0^{(1)}\left(k\sqrt{(x+\xi)^2+(y-\zeta)^2}\right)$$

this latter field (source plus image) being chosen as it satisfies the reflecting-shoreline condition.

If we use the second matching condition, (8), and orthogonality of $\{\cos\lambda_n^{s}y\}$ and $\{\sin\lambda_n^{a}y\}$ in turn, we obtain the same systems of algebraic equations as before, except we obtain different (but equivalent) expressions for the matrix elements; these are

$$\begin{aligned}D_{mn}^{s} &= \frac{1}{2}\int_{-b}^{b}\int_{-b}^{b} H_0^{(1)}(k|y-\zeta|)\cos\lambda_m^{s}y\cos\lambda_n^{s}\zeta\,d\zeta\,dy \\ D_{mn}^{a} &= \frac{1}{2}\int_{-b}^{b}\int_{-b}^{b} H_0^{(1)}(k|y-\zeta|)\sin\lambda_m^{a}y\sin\lambda_n^{a}\zeta\,d\zeta\,dy\end{aligned} \tag{25}$$

These expressions, being double integrals, are less convenient for numerical computations than the single integrals given in Appendix A.

2.4 Plane wave approximation

The plane wave approximation, based on taking only a single symmetric propagating (dominant) mode in the channel, can provide a reasonably accurate solution with far less computational effort than the full solutions outlined above, particularly for small values of kb. Here, ϕ_1 will remain as given in (21), while ϕ_2 is taken simply as

$$\phi_2 = a_0^{s}e^{ikx} \tag{26}$$

so that we have neglected all the oblique waves in the channel (that is, all terms with $n > 0$ in equation 5 and all terms in (6). Following the same methodology as above, we match the velocities at $x = 0$, obtaining an expression for ϕ_1 in terms of a_0^{s}:

$$\phi_1 = \phi_{\text{inc}} + \phi_{\text{ref}} - \frac{a_0^s k}{2} \int_{-b}^{b} H_0^{(1)}\left(k\sqrt{x^2 + (y-\zeta)^2}\right) \mathrm{d}\zeta \quad (27)$$

which is the same as (23), keeping only the first term in the first summation.

Matching the potentials across the mouth of the channel, leads to

$$a_0^s = 2p\cos(ky\sin\theta) - \frac{a_0^s k}{2} \int_{-b}^{b} H_0^{(1)}(k|y-\zeta|)\,\mathrm{d}\zeta \quad (28)$$

Integrating across the channel and rearranging yields

$$a_0^s = \frac{p\mathcal{L}_0^s(k\sin\theta)}{b + \frac{1}{2}kD_{00}^s} \quad (29)$$

where D_{00}^s is defined as before (25).

For very small arguments, the Hankel function can be approximated as $H_0^{(1)}(x) \sim 1 + 2\mathrm{i}\,(\log(x/2) + \gamma)\,/\pi$, where $\gamma \simeq 0.5772\ldots$ is Euler's constant. With this approximation, D_{00}^s can be determined analytically. The final result, valid for long waves and small channel widths ($kb \ll 1$), is

$$a_0^s = \frac{p\mathcal{L}_0^s(k\sin\theta)/b}{1 + kb\left(\frac{2\mathrm{i}}{\pi}\log(kb) + \Gamma_1\right)} = \frac{2\sin(kb\sin\theta)}{kb\sin\theta\left(1 + kb\left(\frac{2\mathrm{i}}{\pi}\log(kb) + \Gamma_1\right)\right)} \quad (30)$$

where we have defined the (complex) constant

$$\Gamma_1 = 1 - \frac{2\mathrm{i}}{\pi}\left(\frac{3}{2} - \gamma\right)$$

Mei[22] and later McIver & Rawlins[16] used the matched asymptotic expansion method with the assumption of $kb \ll 1$ to solve the same problem. McIver & Rawlins provided both a first and a second order (in kb) solution. In order to compare with their solution, we can rewrite a_0^s to second order in kb and normal incidence as

$$a_0^s = 2p\left(1 - kb\left(\frac{2\mathrm{i}}{\pi}\log kb + \Gamma_1\right) + (kb)^2\left(\frac{2\mathrm{i}}{\pi}\log kb + \Gamma_1\right)^2\right) \quad (31)$$

Their expression differs from a_0^s only in the definition of Γ_1, which they have as

$$\Gamma_1 = 1 - \frac{2\mathrm{i}}{\pi}(1 - \gamma + \log\pi/2)$$

The two values of Γ_1 are quite close, $1 - 0.5566\mathrm{i}$ for ours and $1 - 0.5875\mathrm{i}$ for theirs. These approximations are compared with the eigenfunction solution given by (15) and (20) in Fig. 1, again for normal wave incidence. In the figure, the solid line is the solution obtained using $N = 8$. The dashed line very close to the 'exact' solution corresponds to the plane wave solution (29), which shows very little error. The dotted line is the long plane wave solution, using the small argument form of the Hankel function (30). Finally the lower curve corresponds to the first order solution of McIver & Rawlins, while the upper dashed curve is their second order solution. For small values of kb, say, $kb < 0.4$, their second order solution is better than the long plane wave approximation; however, the exact plane wave solution (29) is better for all kb (due to its different dependency on kb) and retains its validity over the full range of the figure as does the long wave approximation (30). The accuracy of the McIver & Rawlins solution rapidly deteriorates as the assumption of $kb \ll 1$ is violated.

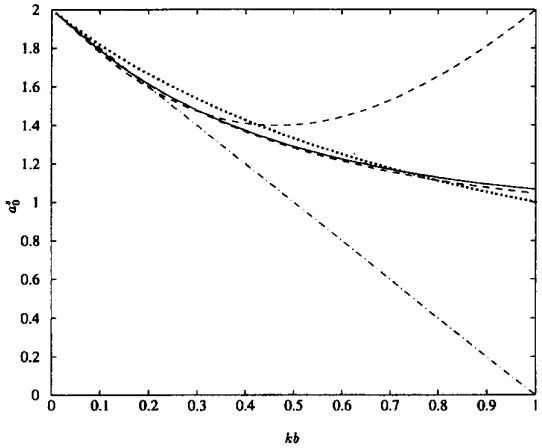

Fig. 1. Approximations and full solution for a_0^s as a function of kb for normal incidence. Solid line is the full solution ($N = 8$), the approximately similar dashed line is the plane wave approximation;[29] the similar dotted line is the long plane wave approximation.[30] The dashed-dotted line corresponds to the McIver & Rawlins' first approximation and the upper dashed line is their second-order solution.

The dependency of long wave approximation of a_0^s (equation 30) on wave angle θ is very weak, as kb is small and the $\sin\theta$ term in the numerator tends to cancel the same term in the denominator.

3 RESULTS

The total velocity potential (obtained by solving the two matrix equations, (15), (20) and adding the results) is readily obtained using a complex matrix solver (we use the IMSL package, LEQT1C, with the Bessel functions computed using the algorithms of Press *et al.*[18]). To obtain the integrals needed for the D_{mn}^{α}, α = s, a, 150 point Gauss quadrature is used. Further, N does not need to be large, if only the first few a_n^{α}s are desired; the coefficient a_m^{α} is quite stable for $N > m+2$. For all results given below, p is taken as unity.

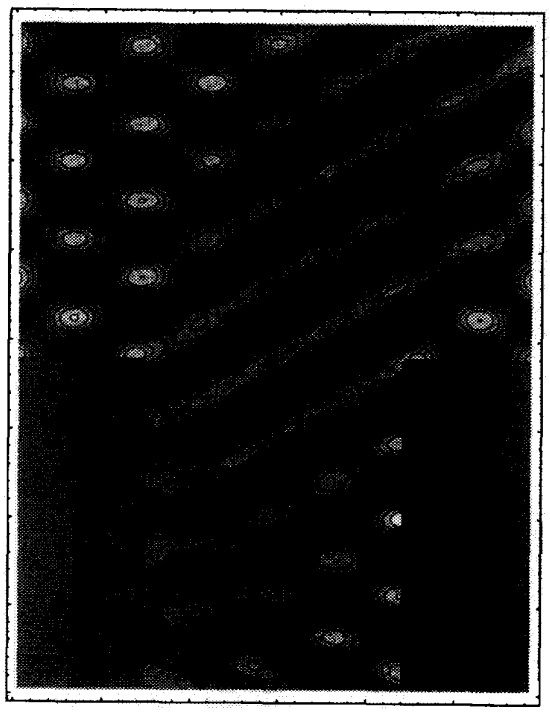

Fig. 2. Instantaneous free surface for thirty degree incident wave train, $kb = 12$.

An overhead view of the instantaneous wave field for a wave train encountering an inlet is shown in Fig. 2 as a shaded contour plot. The wave train is incident from the upper left in the figure at a 30°angle of incidence and reflects from the shoreline, creating a short-crested seastate (maximum amplitude of 2). The wave train propagates into the inlet and reflects from the downwave (right) sidewall. Diffraction of the incident and reflected waves occurs in many locations. Most obvious is the diffraction of the incident wave train from the upwave (left) corner of the inlet within the inlet. However, the seaward propagating waves reflected from the shoreline diffract into the shadow in the reflection pattern caused by the inlet. Further, the reflected wave from the downwave channel sidewall diffracts as well. Here, $kb = 12$, and $N = 16$ for a total of 34 symmetric and antisymmetric modes. Eight of the modes are progressive, four symmetric and four antisymmetric; the remaining 26 modes are evanescent.

Convergence of the assumed series for the potentials (5,6) is predicated on the convergence of the a_n^s and a_n^a for $n = 1, 2, \ldots, N$, as N increases. In Tables 1 and 2, the first three symmetric and antisymmetric (complex) coefficients are shown for N ranging from 4 to 100 for the above example. Due to discontinuities in the velocity profile at the channel mouth and the Gibbs phenomenon occurring with Fourier techniques, the evanescent modal amplitudes decay slowly in magnitude with increasing n for large N; this then results in slight changes in the progressive modes with increasing N. However, if we examine the percentage change in absolute value of a_2^s (the largest modal amplitude) from $N = 4$ to $N = 100$, we find that there is an 0.8 % change. For $N = 16$, the value used for the figure, there is a 0.11% change. It is clear that high N solutions are only incrementally more accurate than $N = 16$; further, the additional evanescent modes decay rapidly away from the channel mouth.

For normal incidence, the instantaneous wave field for $kb = 7.368$, roughly corresponding to one of Melo and Guza's cases, is shown in Fig. 3. For this case, $N = 25$. For this case, as well as the last, the small reflection from the inlet leads to a progressive wave train in front of the inlet in the reflection shadow. Note that there is no focusing after the mouth of the inlet. The normalized velocity across the mouth of the inlet is shown in Fig. 4; it is given in terms of amplitude and phase. At the sides of the channel, the presence of the standing waves along the ocean shoreline creates larger velocities and a phase shift (of about 23°). In the center of the channel the velocities are nearly constant. (Lanczos smoothing (Hamming[24]) is used here for the velocity profile. It removes the high frequency oscillation of the N terms. It was not necessary to use it for the wave field shown above.) Clearly, for a reflective shoreline, it is improper to assume a constant potential or velocity across the mouth of the channel.

The coefficients a_n^s and a_n^a comprising the solutions are functions of kb (the channel width normalized by the wavelength), and the wave angle of incidence. Figure 5 shows the $|a_n^s|$, $n = 0, 1, 2$ for normal incidence ($\theta = 0$) and $p = 1$. The upper solid line in the figure depicts $|a_0^s|$, obtained from the full solution based on $N = 6$. The neighboring dashed line is $|a_0^s|$ obtained by the plane wave solution. The only discrepancy between the two curves occurs for $1 > kb > 2.5$, which implies that the plane wave approximation is quite good for most values of kb. Both curves show that for a narrow channel ($kb << 1$), $|a_0^s|$ is 2.0, the same height as the standing wave at the reflective shoreline; however, as the channel becomes wider, the wave amplitude drops to unity, as the standing wave at the shoreline has little influence across most of the mouth of the channel. The lower dashed line in the same figure corresponds to $|a_1^s|$, which reaches its maximum at $kb = \pi$. In fact for normal incidence, the maxima for $|a_n^s|s$ occur at $kb = n\pi$.

For an incident wave angle of 45°, the modal amplitudes are significantly different. The $|a_n s|s$, $n = 0, 1, 2, 3$ are shown in Fig. 6. Again the plane wave solution for $|a_0^s|$ is plotted along with the full solution with very little discrepancy between the two. As the wave length becomes shorter with respect to the channel width (kb larger), the higher channel modes exceed the fundamental mode in magnitude. Maxima for each $|a_m^s|$ occur at $k \sin\theta = \lambda_m^s = m\pi/b$.

The corresponding antisymmetric modal amplitudes a_n^a for this case are shown in Fig. 7. The peaks for the mth mode occur at $k \sin\theta = \lambda_m^a = (n + \frac{1}{2})\pi/b$.

Figure 8 shows the fundamental mode amplitude $|a_0^s|$ as a function of kb and θ. The upper left edge of the draw-

Table 1. Symmetric modal amplitudes, a_n^s, $n = 0, 1, 2$ for different values of N for $kb = 12$ and $\theta = 30°$

N	a_0^s	a_1^s	a_2^s
2	$-4.82835\times10^{-02} + 8.02038\times10^{-03}$i	$0.131986 - 1.67377\times10^{-02}$i	$0.959272 + 1.91355\times10^{-02}$i
4	$-5.03636\times10^{-02} + 1.21041\times10^{-02}$i	$0.136314 - 2.54473\times10^{-02}$i	$0.954346 + 3.00230\times10^{-02}$i
8	$-4.88583\times10^{-02} + 1.40675\times10^{-02}$i	$0.133097 - 2.94901\times10^{-02}$i	$0.958356 + 3.44728\times10^{-02}$i
12	$-4.83347\times10^{-02} + 1.43210\times10^{-02}$i	$0.132011 - 2.99970\times10^{-02}$i	$0.959585 + 3.49780\times10^{-02}$i
16	$-4.80901\times10^{-02} + 1.43944\times10^{-02}$i	$0.131507 - 3.01422\times10^{-02}$i	$0.960142 + 3.51176\times10^{-02}$i
20	$-4.79520\times10^{-02} + 1.44225\times10^{-02}$i	$0.131224 - 3.01973\times10^{-02}$i	$0.960452 + 3.51691\times10^{-02}$i
50	$-4.76622\times10^{-02} + 1.44446\times10^{-02}$i	$0.130631 - 3.02391\times10^{-02}$i	$0.961094 + 3.52030\times10^{-02}$i
100	$-4.75747\times10^{-02} + 1.44422\times10^{-02}$i	$0.130452 - 3.02337\times10^{-02}$i	$0.961287 + 3.51954\times10^{-02}$i

Table 2. Antisymmetric modal amplitudes, a_n^a, $n = 0, 1, 2$ for different values of N for $kb = 12$ and $\theta = 30°$

N	a_0^a	a_1^a	a_2^a
2	$2.34564\times10^{-02} - 0.342317$i	$-2.60223\times10^{-02} + 0.833990$i	$3.45957\times10^{-02} + 0.449957$i
4	$1.49803\times10^{-02} - 0.339053$i	$-1.64364\times10^{-02} + 0.830156$i	$2.14719\times10^{-02} + 0.455746$i
8	$1.27827\times10^{-02} - 0.338360$i	$-1.40667\times10^{-02} + 0.829286$i	$1.86336\times10^{-02} + 0.457186$i
12	$1.20915\times10^{-02} - 0.338155$i	$-1.33343\times10^{-02} + 0.829040$i	$1.77854\times10^{-02} + 0.457555$i
16	$1.17660\times10^{-02} - 0.338066$i	$-1.29907\times10^{-02} + 0.828936$i	$1.73898\times10^{-02} + 0.457706$i
20	$1.15800\times10^{-02} - 0.338019$i	$-1.27948\times10^{-02} + 0.828881$i	$1.71648\times10^{-02} + 0.457783$i
50	$1.11799\times10^{-02} - 0.337933$i	$-1.23738\times10^{-02} + 0.828782$i	$1.66824\times10^{-02} + 0.457919$i
100	$1.05270\times10^{-02} - 0.337888$i	$-1.16904\times10^{-02} + 0.828734$i	$1.59083\times10^{-02} + 0.457975$i

ing corresponds to 0° of incidence, the same as shown in Fig. 5. A transect from upper right to lower left through the middle of the figure would correspond to Fig. 6. The kinks in the surface that are particularly evident at the 90° angle of incidence correspond to multiples of π. Figures 9 and 10 show the higher symmetric modes, $|a_1^s|$ and $|a_2^s|$ in the same way. Note that higher modes look very similar, just displaced by multiples of π along the kb axis. Figures 11, 12 and 13 show the antisymmetric modes, also as a function of kb and θ.

These figures of modal amplitudes provide information concerning the importance of each of the modes in a particular case. For example, for Fig. 2, corresponding to a 30° angle of incidence and $kb = 12$, the first important symmetric mode is a_2^s, while all the antisymmetric modes shown (a_0^a–a_2^a) are important. For Fig. 3, the a_0^s mode is the most important, due to the normal incidence of the waves, and all the antisymmetric modes are zero.

The energy flux into the channel, relative to the flux on the inlet due to a plane wave at normal incidence, $\mathcal{T}_E$, is a measure of how much energy is transmitted into the bay. This quantity can be calculated from Stoker[25] (see page 48 of that reference):

$$\mathcal{T}_E = \frac{1}{2kb}\mathrm{Im}\left(\int_{-b}^{b} \phi_2^*(\ell, y)\frac{\partial\phi_2}{\partial x}(\ell, y)\,\mathrm{d}y\right)$$

where the asterisk denotes complex conjugation. Due to the orthogonality of the eigenfunctions across the channel this quantity can be separated into symmetric and antisymmetric parts

$$\mathcal{T}_E = \mathcal{T}_E^s + \mathcal{T}_E^a \tag{32}$$

where

$$\mathcal{T}_E^s = |a_0^s|^2 + \tfrac{1}{2}\sum_{n=1}^{\infty}\mathrm{Re}\left(\frac{\beta(\lambda_n^s)}{k}\right)|a_n^s|^2 \tag{33}$$

$$\mathcal{T}_E^a = \tfrac{1}{2}\sum_{n=0}^{\infty}\mathrm{Re}\left(\frac{\beta(\lambda_n^a)}{k}\right)|a_n^a|^2 \tag{34}$$

Note that the above sums involve only a finite number of terms, corresponding to the allowable propagating modes in the channel for which β is real. Figure 14 shows $\mathcal{T}_E$ as a function of the angle of incidence (0°-90°) and the relative width of the channel. For small channel widths, the value of $\mathcal{T}_E$ approaches 4, as the wave amplitude in the channel is 2 due to the standing waves at the ocean shoreline.

4 CONCLUSIONS

The wave field in the vicinity of an inlet allowing for diffraction and reflection has been obtained. A plane wave approximation is shown to provide accurate values for the normal wave mode in the channel, better for small kb than those solutions obtained by matched asymptotic expansions. This plane wave solution (29) is shown to be valid for large values of kb as well, when the other wave modes become important.

The full solution, truncated to N symmetric and antisymmetric modes, has been examined to find the dependency of wave modes on channel size (kb) and angle of incidence. Cross channel responses to external wave forcing can be quite large when $k\sin\theta$ is a multiple of π (symmetric mode) or $\pi/2$ (antisymmetric mode).

The case examined here is simple in geometry and the results provide test cases and guidance for numerical models for more complicated situations. Changing the slope of the side walls (say as in Dalrymple *et al.*[26])

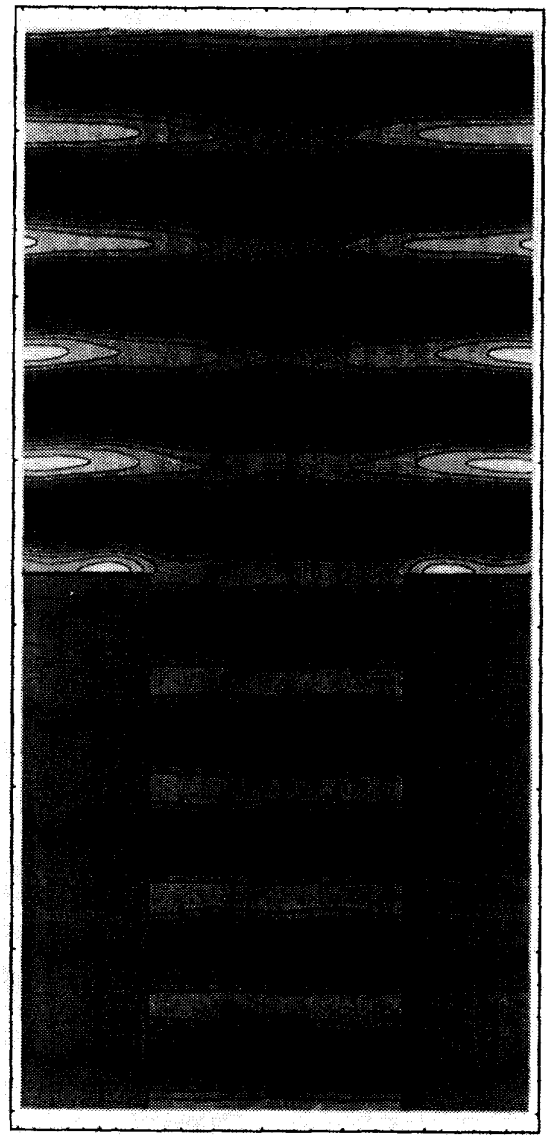

Fig. 3. Instantaneous free surface for normally incident wave train, kb= 7.368.

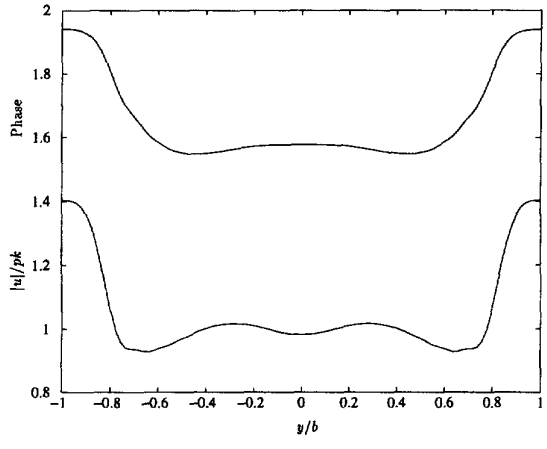

Fig. 4. Dimensionless velocity (x direction) across the mouth of the channel. Lower curve is $|u(0, y)|$, while the upper curve is the phase angle.

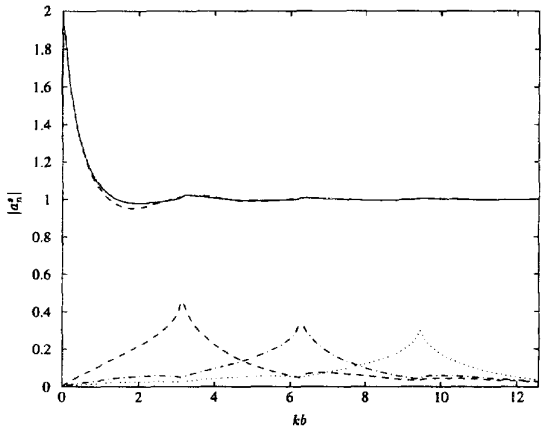

Fig. 5. Symmetric modal amplitudes as a function of dimensionless channel width for normal incidence. The solid line corresponds to $|a_0^s|$, obtained via the full solution, while the nearly identical dashed line is obtained from the plane wave approximation. The lower dashed line is $|a_1^s|$, the dashed-dotted line is $|a_2^s|$, and the dotted line is $|a_3^s|$.

can lead to amplification of the wave motion at the still water line by the presence of edge waves. Large damping may occur within the channel for roughened or porous sidewalls as mentioned in the Introduction.

ACKNOWLEDGEMENTS

The first author's portion of this paper was partially funded by the NOAA Office of Sea Grant, Department of Commerce Under Grant No. NA16RG0162-02 (R/OE 12 and R/OE 13), administered through the University of Delaware Sea Grant Program. The US Government is authorized to produce and distribute reprints for government purposes notwithstanding any copyright notation that may appear herein.

REFERENCES

1. Melo, E. and Guza, R. T., Wave propagation in a jettied entrance channel, I: Models. *J. Waterway, Port, Coastal & Ocean Engng*, **117** (1991) 471–92.
2. Melo, E. and Guza, R. T., Wave propagation in a jettied entrance channel, II: Observations. *J. Waterway, Port, Coastal & Ocean Engng*, **117** (1991) 493–510.
3. Dalrymple, R. A., Water wave propagation in jettied channels. *Proc. 23rd Int. Conf. Coastal Engineering* (1992) 3040–53.
4. Martin, P. A. and Dalrymple, R. A., On the propagation of water waves along a porous-walled channel. *Proc. R. Soc. London, Series A*, **444** (1994) 411–28.
5. Kirby, J. T., Dalrymple, R. A. and Kaku, H., Parabolic approximations for water waves in conformal coordinate systems. *Coastal Engng*, **23** (1994) 185–213.
6. Dalrymple, R. A., Kirby, J. T. and Martin, P. A., Spectral methods for forward-propagating water waves in

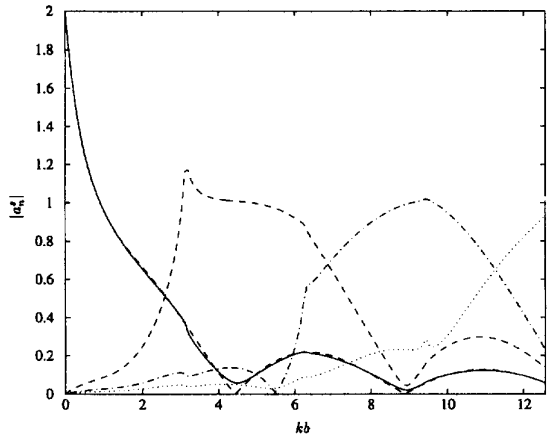

Fig. 6. Symmetric modal amplitudes as a function of dimensionless channel width for 45°incidence. The solid line corresponds to $|a_0^s|$, obtained via the full solution, while the nearly identical dashed line is obtained from the plane wave approximation. The lower dashed line is $|a_1^s|$, the dashed-dotted line is $|a_2^s|$, and the dotted line is $|a_3^s|$.

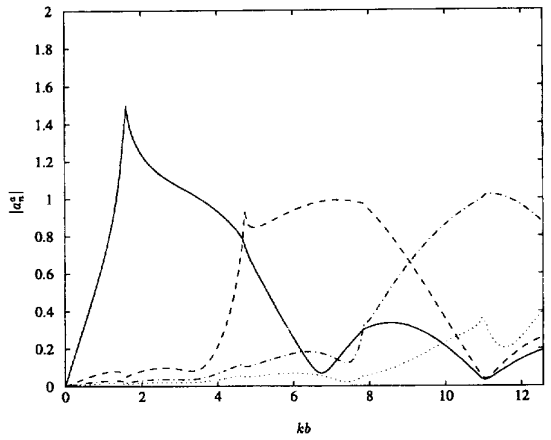

Fig. 7. Antisymmetric modal amplitudes as a function of dimensionless channel width For 45°incidence. The solid line corresponds to $|a_0^a|$. The lower dashed line is $|a_1^a|$, the dashed-dotted line is $|a_2^a|$, and the dotted line is $|a_a|$.

conformally-mapped channels. *Appl. Ocean Res.*, **16** (1994) 249–66.

7. Momoi, T., A long wave in the vicinity of an estuary [I]—an analysis by the method of the buffer domain. *Bull. Earthquake Inst.*, **43** (1965) 291–316.
8. Momoi, T., A long wave in the vicinity of an estuary [II]—an analysis by the method of the buffer domain. *Bull. Earthquake Inst.*, **43** (1965) 459–98.
9. Momoi, T., A long wave in the vicinity of an estuary [III]–an analysis by the method of the buffer domain. *Bull. Earthquake Inst.*, **44** (1966) 1009–40.
10. Momoi, T., A long wave in the vicinity of an estuary [IV]. *Bull. Earthquake Inst.*, **46** (1968) 631–50.
11. Takano, K., Effets d'un obstacle parallelepipedique sur la propagation de la houle. *La Houille Blanche*, **15** (1960) 247–67.
12. Newman, J. N., Propagation of water waves over an infinite

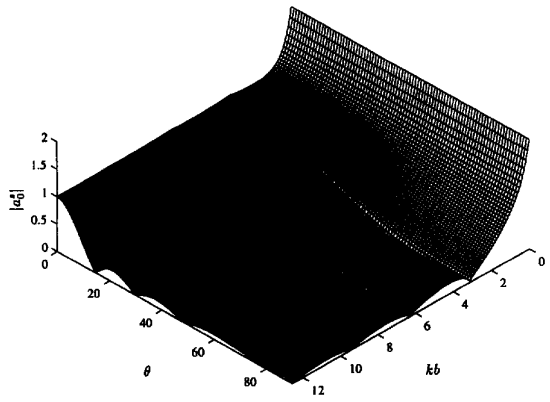

Fig. 8. $|a_0^s|$ as a function of dimensionless channel width and angle of incidence.

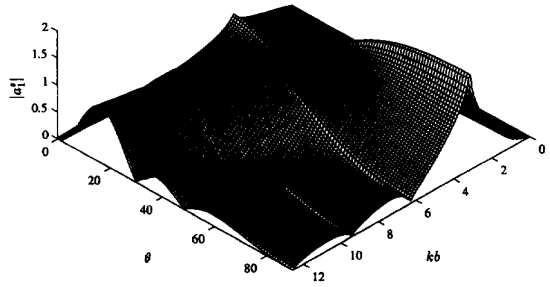

Fig. 9. $|a_1^s|$ as a function of dimensionless channel width and angle of incidence.

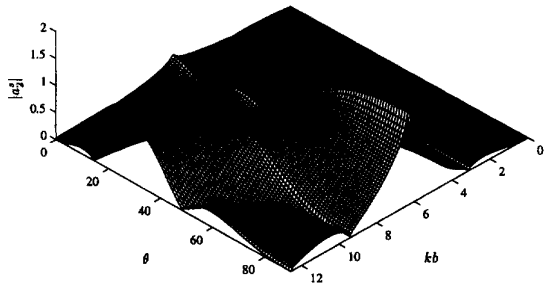

Fig. 10. $|a_2^s|$ as a function of dimensionless channel width and angle of incidence.

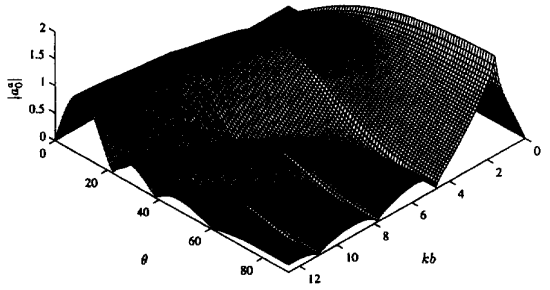

Fig. 11. $|a_0^a|$ as a function of dimensionless channel width and angle of incidence.

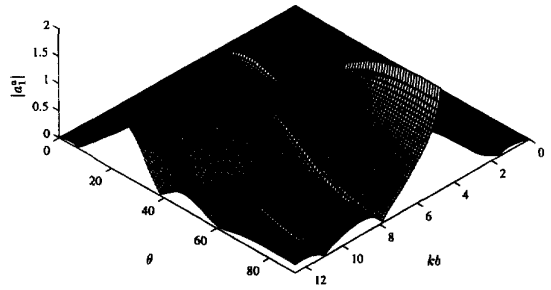

Fig. 12. $|a_1^a|$ as a function of dimensionless channel width and angle of incidence.

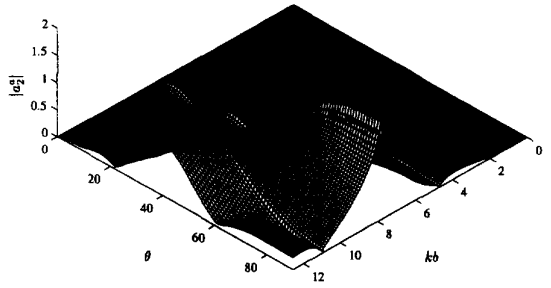

Fig. 13. $|a_2^a|$ as a function of dimensionless channel width and angle of incidence.

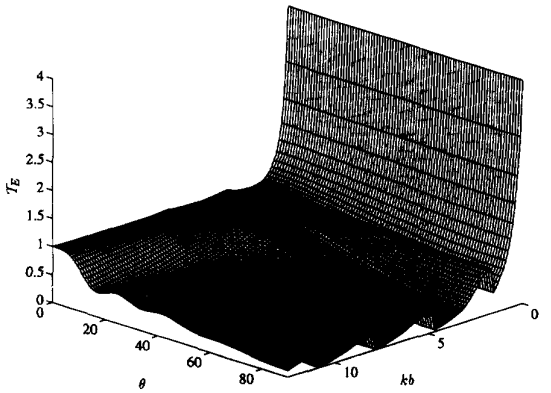

Fig. 14. Transmitted energy flux as a function of dimensionless channel width and angle of incidence.

step. *J. Fluid Mech.*, **23** (1965) 299–415.
13. Havelock, T. H., Forced surface waves on water. *Phil. Mag.*, **7** (1929) 569–76.
14. Dalrymple, R. A. and Martin, P. A., Wave diffraction through offshore breakwaters. *J. Waterway, Port, Coastal & Ocean Engng*, **116** (1990) 727–41.
15. Dalrymple, R. A. and Kirby, J. T., Angular spectrum modeling of water waves. *Rev. Aquatic Sci.*, **6** (1992) 383–404.
16. McIver, P. and Rawlins, A. D., Two-dimensional wave scattering problems involving parallel-walled ducts. *Quart. J. Mech. Appl. Math.*, **46** (1993) 89–116.
17. Miles, J. W., The coupling of a cylindrical tube to a half-infinite space. *J. Acoust. Soc. Amer.*, **20** (1948) 652–64.
18. Chester, W., The propagation of sound waves in an open-ended Channel. *Phil. Mag.*, **41** (1950) 11–33.
19. Scharstein, R. W., Two numerical solutions for the parallel plate-fed slot antenna. *IEEE Trans. Antennas & Prop.*, **37** (1989) 1415–26.
20. Kabalan, K. Y. and El-Haji, A., Characteristic mode formulation of the aperture-fed waveguide problem. *Archiv für Electronik und Übertragungstechnik (AEÜ)*, **48** (1994) 130–4.
21. Dalrymple, R. A. and Greenberg, M. D., Directional wave makers. In *Physical Modelling in Coastal Engineering*, ed. R. A. Dalrymple. A. A. Balkema, Rotterdam, 1984, pp.67–79.
22. Mei, C. C., *The Applied Dynamics of Ocean Surface Waves.* Wiley-Interscience, New York, 1983, 740pp.
23. Press, W. H., Teukolsky, S. A., Vetterline, W. T. and Flannery, B. P., *Numerical Recipes in FORTRAN*, 2nd edn., Cambridge University Press, 1992, 963pp.
24. Hamming, R. W., *Numerical Methods for Scientists and Engineers*, 2nd edn., McGraw-Hill, New York, 1973, 721 pp.
25. Stoker, J. J. *Water Waves: The Mathematical Theory with Applications*, Wiley-Interscience, New York, 1958, 567pp.
26. Dalrymple, R. A., Kirby, J. T. and Li, L., The propagation of water waves in channels. *Proc. Int. Symp. on Waves*, IAHR, Vancouver (1994) 570–9.

APPENDIX A: EVALUATION OF D^s_{MN} AND D^a_{MN}

From (12) and (14), we have

$$\mathrm{Re}\, D^s_{mn} = \frac{4(-1)^{m+n}}{\pi K^2} \int_0^1 \frac{\mu^2 \sin^2 K\mu}{(\mu^2 - (\mu^s_m)^2)(\mu^2 - (\mu^s_n)^2)} \frac{\mathrm{d}\mu}{\sqrt{1-\mu^2}}$$

$$\mathrm{Im}\, D^s_{mn} = \frac{4(-1)^{m+n+1}}{\pi K^2} \int_1^\infty \frac{\mu^2 \sin^2 K\mu}{(\mu^2 - (\mu^s_m)^2)(\mu^2 - (\mu^s_n)^2)} \frac{\mathrm{d}\mu}{\sqrt{\mu^2-1}}$$

where $K = kb$ and $\mu^s_n = n\pi/K$. Similarly, from (17) and (19), we have

$$\mathrm{Re}\, D^a_{mn} = \frac{4(-1)^{m+n}}{\pi K^2} \int_0^1 \frac{\mu^2 \cos^2 K\mu}{(\mu^2 - (\mu^a_m)^2)(\mu^2 - (\mu^a_n)^2)} \frac{\mathrm{d}\mu}{\sqrt{1-\mu^2}}$$

$$\mathrm{Im}\, D^a_{mn} = \frac{4(-1)^{m+n+1}}{\pi K^2} \int_1^\infty \frac{\mu^2 \cos^2 K\mu}{(\mu^2 - (\mu^a_m)^2)(\mu^2 - (\mu^a_n)^2)} \frac{\mathrm{d}\mu}{\sqrt{\mu^2-1}}$$

where $\mu^a_n = (n + \frac{1}{2})\pi/K$. To simplify these real integrals, we identify two cases, depending on whether $m \neq n$ or $m = n$.

Case I: $m \neq n$

(Note that we allow the possibility that one of m and n is zero). Using partial fractions, we have

$$\mathrm{Re}\, D^\alpha_{mn} = \frac{4(-1)^{m+n}}{\pi K^2[(\mu^\alpha_m)^2 - (\mu^\alpha_n)^2]} \left\{\mu^\alpha_m \tilde{F}^\alpha_m - \mu^\alpha_n \tilde{F}^\alpha_n\right\}$$

$$\mathrm{Im}\, D^\alpha_{mn} = \frac{4(-1)^{m+n+1}}{\pi K^2[(\mu^\alpha_m)^2 - (\mu^\alpha_n)^2]} \left\{\mu^\alpha_m F^\alpha_m - \mu^\alpha_n F^\alpha_n\right\} \quad \text{(A1)}$$

where α = s, a,

$$\tilde{F}_n^{\mathrm{s}} = \mu_n^{\mathrm{s}} \int_0^1 \frac{\sin^2 K\mu}{\mu^2 - (\mu_n^{\mathrm{s}})^2} \frac{\mathrm{d}\mu}{\sqrt{1-\mu^2}}$$

$$F_n^{\mathrm{s}} = \mu_n^{\mathrm{s}} \int_1^\infty \frac{\sin^2 K\mu}{\mu^2 - (\mu_n^{\mathrm{s}})^2} \frac{\mathrm{d}\mu}{\sqrt{\mu^2-1}}$$

$$\tilde{F}_n^{\mathrm{a}} = \mu_n^{\mathrm{a}} \int_0^1 \frac{\cos^2 K\mu}{\mu^2 - (\mu_n^{\mathrm{a}})^2} \frac{\mathrm{d}\mu}{\sqrt{1-\mu^2}}$$

$$F_n^{\mathrm{a}} = \mu_n^{\mathrm{a}} \int_1^\infty \frac{\cos^2 K\mu}{\mu^2 - (\mu_n^{\mathrm{a}})^2} \frac{\mathrm{d}\mu}{\sqrt{\mu^2-1}}$$

For $\tilde{F}_n^\alpha$, the integrand has a removable singularity at $\mu = \mu_n^\alpha$, if $0 \le \mu_n^\alpha \le 1$. It also has a square-root singularity at $\mu = 1$; this can be eliminated using the substitution $\mu = \sin\theta$. We can rewrite F_n^α as an integral over a finite range as follows. First, we use partial fractions again to obtain

$$F_n^\alpha = \tfrac{1}{2} L(K, \mu_n^\alpha) - \tfrac{1}{2} L(K, -\mu_n^\alpha), \tag{A2}$$

where

$$L(K,\nu) = \int_1^\infty \frac{\sin^2[K(\mu-\nu)]}{\mu-\nu} \frac{d\mu}{\sqrt{\mu^2-1}}$$

and, making use of the definitions of μ_n^{s} and μ_n^{a}, we have

$$\sin^2 K\mu = \sin^2[K(\mu \pm \mu_n^{\mathrm{s}})],$$
$$\cos^2 K\mu = \sin^2[K(\mu \pm \mu_n^{\mathrm{a}})].$$

Next, we consider K and ν as independent variables, so that

$$\frac{\partial L}{\partial K}(K,\nu) = \int_1^\infty \sin[2K(\mu-\nu)] \frac{\mathrm{d}\mu}{\sqrt{\mu^2-1}}$$
$$= \tfrac{1}{2}\pi \{J_0(2K)\cos(2K\nu) + Y_0(2K)\sin(2K\nu)\}$$

using standard integrals for the Bessel functions J_0 and Y_0. Integrating, using $L(0,\nu) = 0$, gives

$$L(K,\nu) = \tfrac{1}{2}\pi K \int_0^1 \{J_0(2Ks)\cos(2K\nu s) + Y_0(2Ks)\sin(2K\nu s)\}\,\mathrm{d}s$$

Setting $\nu = \pm\mu_n^\alpha$, and substituting into (A2) gives

$$F_n^{\mathrm{s}} = F_{2n} \quad \text{and} \quad F_n^{\mathrm{a}} = F_{2n+1}, \tag{A3}$$

where $F_m(K)$ is defined by

$$F_m = \tfrac{1}{2}\pi K \int_0^1 Y_0(2Ks)\sin(m\pi s)\,\mathrm{d}s$$

whence $\operatorname{Im} D_{mn}^\alpha$ is given by (A1).

Case II: $m = n$

From (12), (17), (14) and (19), we have

$$\operatorname{Re} D_{nn}^{\mathrm{s}} = \frac{4}{\pi K^2} \int_0^1 \left(\frac{\mu \sin K\mu}{\mu^2 - (\mu_n^{\mathrm{s}})^2} \right)^2 \frac{\mathrm{d}\mu}{\sqrt{1-\mu^2}}$$

$$\operatorname{Re} D_{nn}^{\mathrm{a}} = \frac{4}{\pi K^2} \int_0^1 \left(\frac{\mu \cos K\mu}{\mu^2 - (\mu_n^{\mathrm{a}})^2} \right)^2 \frac{\mathrm{d}\mu}{\sqrt{1-\mu^2}}$$

for $n \ge 0$; these integrals do not seem to simplify further. For $\operatorname{Im} D_{nn}^\alpha$, we start with

$$\frac{4\mu^2}{(\mu^2 - (\mu_n^\alpha)^2)^2} = \frac{1}{(\mu-\mu_n^\alpha)^2} + \frac{1}{(\mu+\mu_n^\alpha)^2} + \frac{2}{\mu^2 - (\mu_n^\alpha)^2}$$

for $\alpha = \mathrm{s}, \mathrm{a}$. Apart from the case $n = 0$ and $\alpha = \mathrm{s}$, we have

$$\operatorname{Im} D_{nn}^\alpha = -(\pi K^2)^{-1}\{M(K,\mu_n^\alpha) + M(K,-\mu_n^\alpha) + (2/\mu_n^\alpha)F_n^\alpha\} \tag{A4}$$

where F_n^α is given by (A3) and

$$M(K,\nu) = \int_1^\infty \frac{\sin^2[K(\mu-\nu)]}{(\mu-\nu)^2} \frac{\mathrm{d}\mu}{\sqrt{\mu^2-1}}$$

We proceed as for $L(K,\nu)$, except that now we differentiate twice to give

$$\frac{\partial^2 M}{\partial K^2}(K,\nu) = 2\int_1^\infty \cos[2K(\mu-\nu)] \frac{\mathrm{d}\mu}{\sqrt{\mu^2-1}}$$
$$= \pi\{J_0(2K)\sin(2K\nu) - Y_0(2K)\cos(2K\nu)\}$$

Integrating twice, using $M = \partial M/\partial K = 0$ at $K = 0$, gives

$$M(K,\nu) = \pi K^2 \int_0^1 (1-s)\{J_0(2Ks)\sin(2K\nu s) - Y_0(2Ks)\cos(2K\nu s)\}\,\mathrm{d}s$$

Hence, (A4) gives

$$\operatorname{Im} D_{nn}^{\mathrm{s}} = E_{2n} \quad \text{and} \quad \operatorname{Im} D_{nn}^{\mathrm{a}} = E_{2n+1}, \tag{A5}$$

where $E_m(K)$ is defined by

$$E_m = 2\int_0^1 Y_0(2Ks)\left\{(1-s)\cos(m\pi s) - \frac{\sin(m\pi s)}{m\pi}\right\}\mathrm{d}s$$

The first equation in (A5) is not valid when $n = 0$; in this case, we have

$$\operatorname{Im} D_{00}^{\mathrm{s}} = \frac{-4}{\pi K^2} M(K,0) = 4\int_0^1 (1-s)Y_0(2Ks)\,\mathrm{d}s.$$